Fusion Engineering and Design 221 (2025) 115362

Contents lists available at ScienceDirect

Fusion Engineering and Design

journal homepage: www.elsevier.com/locate/fusengdes

One-dimensional simulations of nonlinear burn control in ITER

Vincent Graber *, Eugenio Schuster

Mechanical Engineering and Mechanics, Lehigh University, Bethlehem, PA 18015, USA

ARTICLE INFO

Keywords:
ITER
Burning plasma
Control-oriented modeling
Plasma simulation
Burn control

ABSTRACT

Actively controlling the plasma temperature and density in future reactor-grade tokamaks will be a formidable challenge due to the multi-dimensional, coupled, and nonlinear characteristics of the burning-plasma dynamics. In ITER, the actuator systems that will be useful for temperature–density control (also known as burn control) include neutral beam injection, ion and electron cyclotron heating, pellet injection, and gas puffing. In this work, a nonlinear, model-based, burn-control algorithm is proposed. A model-based approach is attractive because it directly incorporates the complex plasma dynamics into the burn-control algorithm. Using Lyapunov techniques, the burn-control algorithm is synthesized from a control-oriented plasma model that is zero-dimensional (0-D). The reduced dimensionality of this plasma model renders the burn-control design more feasible. Nonetheless, this 0-D plasma model still captures the nonlinear response of the plasma energy and density to deuterium–tritium (D–T) fusion, radiation, auxiliary heating, external fueling, and other phenomena. More importantly, the control objective is indeed 0-D since the primary goal of a burn controller is usually to regulate volume-averaged properties of the plasma (e.g., overall fusion power P_f or fusion gain Q). This makes 0-D models appropriate for control synthesis. However, the assessment of the effect of the proposed 0-D burn-control algorithms on the spatio-temporal dynamics of the plasma is a critical step of the control-design process. This work presents a one-dimensional (1-D) plasma model that is used in closed-loop simulations. The presented simulation study demonstrates how the spatial profiles of the D–T fuel density, the fusion-born alpha-particle density, the ion energy density, and the electron energy density evolve temporally under 0-D burn control. By testing 0-D controllers in 1-D simulations, the effectiveness of 0-D burn-control techniques can be investigated before implementation in actual tokamaks. Through investigations of this kind, control issues can be identified and addressed, enabling iterative improvement of the burn-control designs.

1. Introduction

The purpose of burn control [1] in fusion reactors like ITER will be to regulate the burning plasma's kinetic properties, namely the temperature and density, in real time. To drive the plasma system to the desired temperature and density, burn controllers rely on a variety of actuator systems that externally heat and fuel the plasma, including the neutral beam injectors, the ion cyclotron system, the electron cyclotron system, the pellet injectors, and the gas valves. Because the fusion power is determined by the plasma's temperature and density, burn control can be used to achieve higher values of Q, which is the ratio between the fusion power output and the auxiliary power put into the plasma. The ITER project seeks to demonstrate the viability of fusion power plants by executing an extended burn with $Q = 10$ [2]. Clearly, burn control will play an important role in completing ITER's objectives.

The advantage of a model-based approach to burn control is that it directly incorporates the highly complex plasma dynamics in the control algorithm [3,4]. In prior work [5], burn controllers were synthesized from control-oriented models using Lyapunov techniques [6]. These control-oriented models were zero-dimensional (0-D), which made it more feasible to derive the model-based burn control laws. Even with their reduced dimensionality, these 0-D models still capture the nonlinear and coupled dynamics of the burning plasma. Regardless of the practicalities of control synthesis, 0-D models are very appropriate for burn control design. This is because the primary goal of burn control is the regulation of *volume-averaged* plasma properties (e.g., energy and density). Indeed, the ITER project's objective of achieving $Q = 10$ is 0-D.

Ahead of its construction, the burning plasma transport in ITER is not entirely known. Under this uncertainty, adaptive control techniques [7] are attractive. By estimating parameters that are considered to be uncertain (i.e., they are not precisely known) in the control-orientated model, adaptive controllers *adapt* the control laws in real

* Corresponding author.
E-mail address: graber@lehigh.edu (V. Graber).

https://doi.org/10.1016/j.fusengdes.2025.115362
Received 16 January 2025; Received in revised form 17 June 2025; Accepted 21 July 2025
Available online 6 August 2025

time to improve their performance under the current plasma conditions. Before ITER implementation, the aforementioned adaptive burn control algorithms [5] should be evaluated in plasma simulations that have a higher-fidelity than the control-oriented models used to derive them. With their capability to adapt online, adaptive burn controllers should be particularly adept in the uncertain environment of a higher-fidelity simulation.

In the prior work [5], the proposed adaptive burn controllers were evaluated in 0-D simulations. Although this work presents an adaptive burn controller that is similar to those found in this prior work, this work extends previous efforts by presenting a one-dimensional (1-D) plasma model that is used to test the burn controller in closed-loop simulations. The presented simulation study demonstrates how the plasma's kinetic profiles evolve temporally under 0-D burn control. Through studies of this kind, the capability of the model-based burn control can be assessed and improved upon before implementation in actual tokamaks.

A key contribution of this work is indeed a 1-D numerical code, which is an upgrade to the control-oriented plasma transport simulator COTSIM [8,9], that enables closed-loop burn control simulations. The 1-D code solves separate transport equations for the ion temperature, the electron temperature, and all of the ion species (deuterium, tritium, alpha-particles, and impurities). Furthermore, COTSIM can run faster than real time, and it is specifically designed to support complex, nonlinear feedback-control laws. Therefore, the 1-D code presented in this work is suitable for the kind of iterative burn control design that should be initiated ahead of ITER operation. Other fast tokamak simulators include RAPTOR [10] and METIS [11], which was originally a module for a suite of codes called CRONOS [12]. Kinetic control with pellet injection has been studied for EU-DEMO [13] using the so-called "tokamak flight simulator" Fenix [14], which incorporates the 1-D transport code ASTRA [15].

This paper is organized as follows. The control-oriented, 0-D model of the burning plasma is presented in Section 2. In Sections 3 and 4, control objectives are drawn and the 0-D plasma model is used to synthesize a nonlinear burn controller. Then, the 1-D burning plasma model is presented in Section 5. Section 6 explains how the aforementioned 0-D burn controller is implemented in the 1-D simulation study presented in Section 7. Finally, conclusions and potential future work are discussed in Section 8.

2. The 0-D plasma model for control synthesis

In this section, the 0-D plasma model is presented. Although this 0-D model is very similar to that presented in prior work [5], it is provided here in its entirety because Sections 3–6 make several references to the equations presented in this section. Both the control objectives (Section 3) and the control laws (Section 4) are based on the 0-D model's equations. More importantly, the 1-D plasma model (Section 5) shares some equations with the 0-D model. Finally, Section 6 provides an explanation for the implementation of 0-D burn control in 1-D plasma simulations that requires an understanding of both models.

The plasma system includes four ion species: deuterium (D), tritium (T), alpha-particles (α), and impurities (I). The densities of these ion species are governed by

$$\dot{n}_D = -\frac{n_D}{\tau_D} - S_\alpha + S_{aux,D}, \qquad \dot{n}_\alpha = -\frac{n_\alpha}{\tau_\alpha} + S_\alpha, \tag{1}$$

$$\dot{n}_T = -\frac{n_T}{\tau_T} - S_\alpha + S_{aux,T}, \qquad \dot{n}_I = -\frac{n_I}{\tau_I} + S_{sp}, \tag{2}$$

where the notation $\dot{x}$ denotes the time derivative of x such that $\dot{x}=dx/dt$. In (1)–(2), each term is in units of $\mathrm{m^{-3}s^{-1}}$. The burn controller, which is presented in Section 4, provides the commands for the external injection rates of deuterium $S_{aux,D}$ and tritium $S_{aux,T}$.

With the density of each of the ion species defined by (1) and (2), the quasi-neutrality condition defines the electron density as

$$n_e = n_H + 2n_\alpha + Z_I n_I, \tag{3}$$

where $n_H = n_D + n_T$. In (3), Z_I is the average atomic number of the various impurity species within the plasma (excluding the alpha-particles). For ITER, these impurities can include seeded species such as neon or nitrogen [16,17] and eroded tungsten coming from the first wall and divertor [18]. The source of impurities from the plasma-facing components is given by

$$S_{sp} = f_I^{sp} n_e/\tau_E^{sc}, \tag{4}$$

where f_I^{sp} is the sputtering fraction and the energy confinement time τ_E^{sc} is defined later in this section.

Defining the source of alpha-particles, the fusion reaction rate density is given by

$$S_\alpha = n_D n_T \langle\sigma v\rangle \equiv \gamma(1-\gamma) n_H^2 \langle\sigma v\rangle, \tag{5}$$

where the tritium fraction is

$$\gamma = \frac{n_T}{n_H},. \tag{6}$$

In (5), the DT reactivity $\langle\sigma v\rangle$ is a highly nonlinear function of the ion temperature T_i (expressed in keV):

$$\langle\sigma v\rangle = C_1\omega\sqrt{\xi/(m_r c^2 T_i^3)}e^{-3\xi}, \quad \xi = (B_G^2/4\omega)^{1/3},$$
$$\omega = T_i\left[1 - \frac{T_i(C_2 + T_i(C_4 + T_i C_6))}{1 + T_i(C_3 + T_i(C_5 + T_i C_7))}\right]^{-1}, \tag{7}$$

where B_G, $m_r c^2$ and C_j for $j \in \{1,\ldots,7\}$ are constants [19]. This approximate model for S_α assumes that the alpha-particles thermalize instantaneously [3].

Finally, the total ion density, the total plasma density, and the effective atomic number are given by

$$n_i = n_H + n_\alpha + n_I, \tag{8}$$

$$n = n_i + n_e = 2n_H + 3n_\alpha + (Z_I + 1)n_I, \tag{9}$$

$$Z_{eff} = \frac{n_H + 4n_\alpha + Z_I^2 n_I}{n_e}. \tag{10}$$

With each term expressed in units of $\mathrm{W/m^3}$, the ion energy and the electron energy are governed by

$$\dot{E}_i = -\frac{E_i}{\tau_{E,i}} + \phi_\alpha P_\alpha + P_{ei} + P_{aux,i}, \tag{11}$$

$$\dot{E}_e = -\frac{E_e}{\tau_{E,e}} + \bar{\phi}_\alpha P_\alpha - P_{ei} - P_{br} + P_{oh} + P_{aux,e}, \tag{12}$$

where the ion temperature and the electron temperature are given by $T_i = \frac{2}{3}E_i/(n_H + n_\alpha + n_I)$ and $T_e = \frac{2}{3}E_e/n_e$. The controlled auxiliary power is $P_{aux,i}$ and $P_{aux,e}$. The radiation losses, the ohmic heating, and the ion–electron collisional power exchange [2,20] are defined as

$$P_{br} = 5.5\times10^{-37} Z_{eff} n_e^2 \sqrt{T_e}, \tag{13}$$

$$P_{oh} = 2.8\times10^{-9} Z_{eff} I_p^2 a^{-4} T_e^{-3/2}, \tag{14}$$

$$P_{ei} = \frac{3}{2} n_e (T_e - T_i)/\tau_{ei}. \tag{15}$$

In (13) and (14), T_e is expressed in keV, I_p is the plasma current, and a is the plasma minor radius. In (15), the energy relaxation time is given by

$$\tau_{ei} = \frac{3\pi\sqrt{2\pi}\epsilon_0^2 T_e^{3/2}}{e_c^4 m_e^{1/2} \ln\Lambda_e} \sum_p \frac{m_p}{n_p Z_p^2} \quad \text{for } p \in \{D, T, \alpha, I\}, \tag{16}$$

where $e_c = 1.622\times10^{-19}$ C, $m_e = 9.1096\times10^{-31}$ kg, $\epsilon_0 = 8.854\times10^{-12}$ F/m, and T_e is expressed in J. In the summation, m_p, n_p, and Z_p are the mass, density, and atomic number of each ion species. The natural logarithm is given by $\Lambda_k = 1.24\times10^7 T_k^{3/2}/(n_k^{1/2} Z_{eff}^2)$ for $k \in \{i, e\}$ where T_k is in units of K.

The alpha-particle power is defined as $P_\alpha = E_\alpha S_\alpha$ where S_α is given by (5) and $E_\alpha = 3.52$ MeV. The fraction of P_α deposited into the plasma's ion population is given by

$$\phi_\alpha = \frac{1}{x_0}\left[\frac{1}{3}\ln\frac{1-x_0^{\frac{1}{2}}+x_0}{(1+x_0^{\frac{1}{2}})^2} + \frac{2}{\sqrt{3}}\left(\tan^{-1}\frac{2x_0^{\frac{1}{2}}-1}{\sqrt{3}}+\frac{\pi}{6}\right)\right], \tag{17}$$

where $x_0 = \varepsilon_{\alpha_0}/\varepsilon_c$ is the ratio between the alpha-particle's initial kinetic energy ($\varepsilon_{\alpha_0} = E_\alpha$) and the critical energy. The critical energy [21] is defined as

$$\varepsilon_c = m_e^{-1/3} A_\alpha \frac{T_e}{n_e^{2/3}}\left(\frac{3\sqrt{\pi}\ln\Lambda_i}{4\ln\Lambda_e}\right)^{2/3}\left(\sum_p \frac{n_p Z_p^2}{A_p}\right), \tag{18}$$

for $p \in \{D,T,\alpha,I\}$. In (18), m_e is expressed in amu, and A_p is the atomic mass of each ion species (e.g., $A_\alpha = 4$). A derivation of (17) can be found in [22]. The fraction of P_α deposited into the electrons is $\bar{\phi}_\alpha = 1-\phi_\alpha$.

The global energy confinement time [23,24] is given by $\tau_E = H\tau_E^{sc}$ where H is a constant and τ_E^{sc} is a scaling law:

$$\tau_E^{sc} = \frac{0.0562 I_p^{0.93} B_T^{0.15} M^{0.19} R^{1.97} \epsilon^{0.58} \kappa^{0.78} n_e^{0.41}}{(P\times V_p)^{0.69}}. \tag{19}$$

For ITER, $I_p = 15$ MA, $B_T = 5.3$ T is the toroidal field, $R=6.2$ m is the plasma major radius, $\epsilon = a/R$, $a = 2$ m, $\kappa=1.7$ is the vertical elongation at 95% flux surface, and $V_p = 757$ m^3 is the total plasma volume. In (19), n_e is expressed in units of 10^{19} m^{-3}, $M = 3\gamma + 2(1-\gamma)$, and the total plasma power (MW/m^3) is given by the power balance: $P = P_{aux,i} + P_{aux,e} - P_{br} + P_\alpha + P_{oh}$. In (1)–(2) and (11)–(12), the confinement times are proportional to the global energy confinement time (τ_E): $\tau_p = k_p\tau_E$ for $p \in \{D,T,\alpha,I\}$ and $\tau_{E,k} = \zeta_k\tau_E$ for $k \in \{i,e\}$.

3. The burn control objectives

The controller will regulate all six states of the nonlinear system ($x = [E_i\ E_e\ n_\alpha\ n_D\ n_T\ n_I]^T$) using the four controlled inputs ($u=[P_{aux,i}\ P_{aux,e}\ S_{aux,D}\ S_{aux,T}]^T$). Tracking all six states is desirable because the fusion power ($P_{fus} = 5\times P_\alpha$) depends on the ion temperature, the fuel density, and the tritium fraction. Therefore, there are several operating points with the same fusion power, and full temperature and density control is required to achieve a particular operating point. The equilibrium values (denoted $\bar{x}$ and $\bar{u}$) can be determined by setting the nonlinear system to steady-state ($d/dt=0$ in (1)–(2) and (11)–(12)) and solving the closed system for the chosen references $r = [\bar{E}_i\ \ \bar{E}_e\ \ \bar{n}\ \ \bar{\gamma}]$. The control objective is to drive the states x to the desired values $\bar{x}$ such that the control error $\tilde{x} = x - \bar{x}$ is brought to zero. The nonlinear system is rewritten such that $\tilde{x} = 0$ is the origin:

$$\dot{\tilde{E}}_i = -\theta_1\frac{\bar{E}_i+\tilde{E}_i}{\tau_E^{sc}} + \phi_\alpha P_\alpha + P_{ei} + P_{aux,i}, \tag{20}$$

$$\dot{\tilde{E}}_e = -\theta_2\frac{\bar{E}_e+\tilde{E}_e}{\tau_E^{sc}} + \bar{\phi}_\alpha P_\alpha - P_{ei} - P_{br} + P_{oh} + P_{aux,e}, \tag{21}$$

$$\dot{\tilde{n}}_\alpha = -\theta_3\frac{\bar{n}_\alpha+\tilde{n}_\alpha}{\tau_E^{sc}} + S_\alpha, \tag{22}$$

$$\dot{\tilde{n}}_D = -\theta_4\frac{\bar{n}_D+\tilde{n}_D}{\tau_E^{sc}} - S_\alpha + S_{aux,D}, \tag{23}$$

$$\dot{\tilde{n}}_T = -\theta_5\frac{\bar{n}_T+\tilde{n}_T}{\tau_E^{sc}} - S_\alpha + S_{aux,T}, \tag{24}$$

$$\dot{\tilde{n}}_I = -\theta_6\frac{\bar{n}_I+\tilde{n}_I}{\tau_E^{sc}} + S_{sp}, \tag{25}$$

where the plasma confinement quality is assumed to be uncertain such that H, ζ_i, ζ_e, k_D, k_T, k_α, and k_I are lumped into $\theta = \left[\theta_1\ \theta_2\ \dots\ \theta_6\right]^T$. The controller's estimate of θ is denoted as $\hat{\theta}$, and the estimation error is $\tilde{\theta} = \hat{\theta} - \theta$.

4. The adaptive burn control laws

In this section, the control laws for u and the adaptive update law for $\hat{\theta}$ are presented. The controller was designed using Lyapunov stability theory [6]. Consider the dynamic system $\dot{y} = f(y)$, which has an equilibrium at the origin. A Lyapunov candidate function $V_y(y)$, which can be viewed as a representation of the system's energy, can be chosen to synthesize a feedback controller. If the controller is designed such that the system's energy is always dissipated ($\dot{V}_y(y) < 0$ for all $y \neq 0$), then the origin is asymptotically stable. Therefore, an asymptotically stabilizing controller can be designed by first choosing an appropriate Lyapunov candidate function $V_y(y)$ and then defining control laws that render $\dot{V}_y(y) < 0$ for all $y \neq 0$.

Consider the following Lyapunov function:

$$V = k_i^2\tilde{E}_i^2 + k_e^2\tilde{E}_e^2 + k_\gamma^2\tilde{\gamma}^2 + \tilde{n}^2 + \tilde{\theta}^T\Gamma_\theta^{-1}\tilde{\theta}, \tag{26}$$

where k_i, k_e, k_γ, and Γ_θ are positive and constant. For brevity, the derivation of the control laws from (26) is omitted from this work. A nearly identical adaptive controller was designed in prior work [5], which includes details on the control synthesis and stability analysis. For this work, the asymptotically stabilizing control laws are

$$P_{aux,i} = \hat{\theta}_1\frac{\bar{E}_i}{\tau_E^{sc}} - \phi_\alpha P_\alpha - P_{ei} - K_I\tilde{E}_i, \tag{27}$$

$$P_{aux,e} = \hat{\theta}_2\frac{\bar{E}_e}{\tau_E^{sc}} - \bar{\phi}_\alpha P_\alpha + P_{ei} + P_{br} - P_{oh} - K_E\tilde{E}_e, \tag{28}$$

$$S_{aux,D} = \frac{1}{2}\left[3\hat{\theta}_3\frac{n_\alpha}{\tau_E^{sc}} + 2\hat{\theta}_4\frac{n_D}{\tau_E^{sc}} + 2\hat{\theta}_5\frac{n_T}{\tau_E^{sc}} + (Z_I+1)\hat{\theta}_6\frac{n_I}{\tau_E^{sc}} \right.$$
$$\left. + S_\alpha - 2S_{aux,T} - (Z_I+1)S_{sp} - K_N\tilde{n}\right], \tag{29}$$

$$S_{aux,T} = \hat{\theta}_5\frac{n_T}{\tau_E^{sc}} + S_\alpha + \gamma\left[\frac{3}{2}\left(\hat{\theta}_3\frac{n_\alpha}{\tau_E^{sc}} - S_\alpha\right) + \frac{(Z_I+1)}{2}\hat{\theta}_6\frac{n_I}{\tau_E^{sc}} \right.$$
$$\left. - \frac{(Z_I+1)}{2}S_{sp} - \frac{K_N}{2}\tilde{n}\right] - K_T\tilde{\gamma}, \tag{30}$$

where K_I, K_E, K_N, and K_T are positive constants. These control laws are augmented with the following adaptive update law that guarantees that the origin is asymptotically stable when the parameters are uncertain ($\hat{\theta} \neq \theta$):

$$\dot{\hat{\theta}} \approx \dot{\tilde{\theta}} = \Gamma_\theta \begin{bmatrix} -(\bar{E}_i/\tau_E^{sc})k_i^2\tilde{E}_i \\ -(\bar{E}_e/\tau_E^{sc})k_e^2\tilde{E}_e \\ -3\tilde{n}(n_\alpha/\tau_E^{sc}) \\ -[2\tilde{n} - ((k_\gamma^2\tilde{\gamma}\gamma)/n_H)](n_D/\tau_E^{sc}) \\ -[2\tilde{n} - (\gamma-1)(k_\gamma^2\tilde{\gamma})/n_H](n_T/\tau_E^{sc}) \\ -\tilde{n}(Z_I+1)(n_I/\tau_E^{sc}) \end{bmatrix}. \tag{31}$$

The approximation $\dot{\hat{\theta}} \approx \dot{\tilde{\theta}}$ is made under the assumption that the uncertain parameters are varying slowly over time in comparison to the system's characteristic time ($\dot{\theta} \approx 0$).

5. The 1-D plasma model for control simulations

Due to the plasma's toroidal symmetry, a coordinate system can be defined on the poloidal cross section [2,25]. As shown in Fig. 1, there are nested toroidal surfaces of constant poloidal magnetic flux. These magnetic flux surfaces are indexed using the mean effective minor radius

$$\rho = \sqrt{\Phi/\pi B_T}, \tag{32}$$

where Φ is the toroidal magnetic flux and B_T is the toroidal field at the magnetic axis. With the normalized radius being defined by $\hat{\rho} = \rho/\rho_b$ where $\rho = \rho_b$ at the last closed flux surface, the domain of the system extends from the magnetic axis at $\hat{\rho} = 0$ to the plasma boundary at $\hat{\rho} = 1$. Using this coordinate system, the transport equations presented

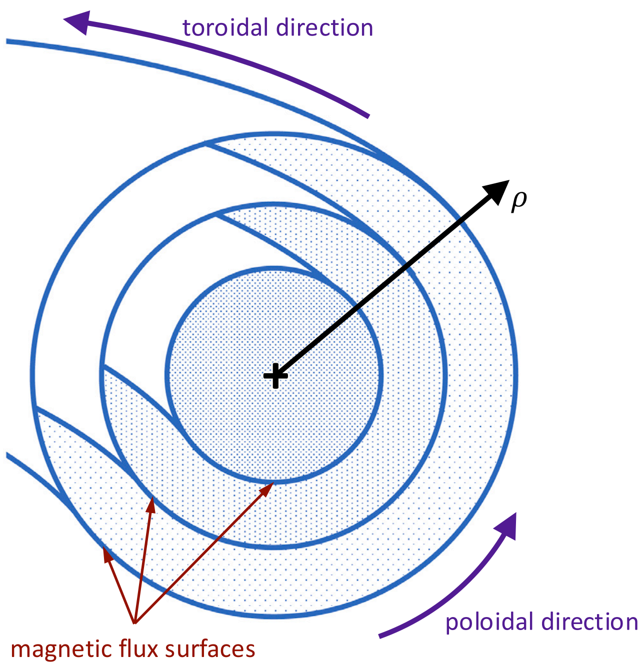

Fig. 1. Cross-sectional view of a tokamak's magnetic configuration where the poloidal magnetic flux is constant on the flux surfaces.

in this section define the 1-D profiles for the ion temperature, electron temperature, deuterium density, tritium density, alpha-particle density, and impurity density.

Similarly to the 0-D density response models (1)–(2), there are four particle transport equations (one for each of the ion species) in the 1-D model. For $p \in \{D, T, \alpha, I\}$,

$$\frac{\partial n_p}{\partial t} = \frac{1}{\rho_b^2 \hat{\rho} \hat{H}} \frac{\partial}{\partial \hat{\rho}}\left[\hat{\rho}\frac{\hat{H}^2 \hat{G}}{\hat{F}} D_p \frac{\partial n_p}{\partial \hat{\rho}}\right] + \Gamma_p^{tot},$$
$$\left.\frac{\partial n_p}{\partial \hat{\rho}}\right|_{\hat{\rho}=0} = 0, \qquad n_p(1,t) = n_p^{bdry}, \tag{33}$$

where each term is in units of $\mathrm{m^{-3}s^{-1}}$ [12,26]. Using the particle transport equations, the 1-D profiles for the ion densities $n_D(\hat{\rho},t)$, $n_T(\hat{\rho},t)$, $n_\alpha(\hat{\rho},t)$, and $n_I(\hat{\rho},t)$ can be solved. The electron density $n_e(\hat{\rho},t)$ and the total ion density $n_i(\hat{\rho},t)$ are defined by (3) and (8), respectively. At the plasma boundary, $n_p^{bdry}(t)$ is the density of a particular ion species. For ion species p, $D_p(\hat{\rho},t)$ is the particle diffusion coefficient. The geometric factors $\hat{F}(\hat{\rho})$, $\hat{G}(\hat{\rho})$, and $\hat{H}(\hat{\rho})$ are related to the configuration of a specific magneto-hydrodynamic (MHD) equilibrium [1]. In (33), the source terms (Γ_p^{tot}) for each of the ion species are

$$\Gamma_D^{tot} = \Gamma_{aux,D} - \Gamma_\alpha, \tag{34}$$
$$\Gamma_T^{tot} = \Gamma_{aux,T} - \Gamma_\alpha, \tag{35}$$
$$\Gamma_\alpha^{tot} = \Gamma_\alpha, \tag{36}$$
$$\Gamma_I^{tot} = \Gamma_{sp}, \tag{37}$$

where $\Gamma_{sp}(\hat{\rho},t)$ and $\Gamma_\alpha(\hat{\rho},t)$ are found by computing (4) and (5) over $\{\hat{\rho} \mid 0 \le \hat{\rho} \le 1\}$. For example, $\Gamma_\alpha(\hat{\rho},t) = n_D(\hat{\rho},t) n_T(\hat{\rho},t) \langle\sigma v\rangle(T_i(\hat{\rho},t))$. The controlled external fueling rates are $\Gamma_{aux,D}(\hat{\rho},t)$ and $\Gamma_{aux,T}(\hat{\rho},t)$.

Similarly to the 0-D energy response models (11)–(12), there are two heat transport equations (one for the ions and one for the electrons) in the 1-D model. For $k \in \{i, e\}$,

$$\frac{3}{2}\frac{\partial}{\partial t}[n_k T_k] = \frac{1}{\rho_b^2 \hat{\rho}\hat{H}}\frac{\partial}{\partial \hat{\rho}}\left[\hat{\rho}\frac{\hat{H}^2\hat{G}}{\hat{F}}\left(\chi_k n_k \frac{\partial T_k}{\partial \hat{\rho}}\right)\right] + Q_k^{tot},$$
$$\left.\frac{\partial T_k}{\partial \hat{\rho}}\right|_{\hat{\rho}=0} = 0, \qquad T_k(1,t) = T_k^{bdry}, \tag{38}$$

where each term is in units of $\mathrm{W/m^3}$ [12,26]. Using the heat transport equations, the radial profiles for the ion temperature $T_i(\hat{\rho},t)$ and the electron temperature $T_e(\hat{\rho},t)$ can be solved. At the plasma boundary, $T_i^{bdry}(t)$ and $T_e^{bdry}(t)$ are the ion and electron temperatures. The thermal diffusion coefficients for the ions and electrons are $\chi_i(\hat{\rho},t)$ and $\chi_e(\hat{\rho},t)$. In (38), the source terms (Q_k^{tot}) for the ions and electrons are

$$Q_i^{tot} = \phi_\alpha Q_\alpha + Q_{ei} + Q_{aux,i}, \tag{39}$$
$$Q_e^{tot} = \bar{\phi}_\alpha Q_\alpha - Q_{ei} - Q_{br} + Q_{oh} + Q_{aux,e}, \tag{40}$$

where $Q_\alpha(\hat{\rho},t) = E_\alpha \Gamma_\alpha$, and the $\phi_\alpha(t)$ is a volume-averaged quantity (17). Respectively, $Q_{br}(\hat{\rho},t)$, $Q_{oh}(\hat{\rho},t)$, and $Q_{ei}(\hat{\rho},t)$ are determined by computing (13), (14), and (15) over the domain $\{\hat{\rho} \mid 0 \le \hat{\rho} \le 1\}$. The controlled auxiliary powers are $Q_{aux,i}(\hat{\rho},t)$ and $Q_{aux,e}(\hat{\rho},t)$.

In this work, the thermal diffusion coefficient for the electrons $\chi_e(\hat{\rho},t)$ ($\mathrm{m^2/s}$) is given by [8,27,28]:

$$\chi_e = F_{CT} \times \left[a_{121}\left(\frac{P_{e,bdry}^{tot}}{n_{e,0}}\right)^{0.6}(RB_T q_{95})^{-0.8} a^{-0.2} + a_{122}\frac{a}{n_{e,0}}(RB_T)^{0.3} Z_{eff}^{0.2}\left(1 + \frac{1}{4}\alpha_n\right) R^{-2.2} q_{95}^{-1.6}\right],$$
$$F_{CT} = 8\pi^2 \frac{P_e^{tot}}{P_{e,bdry}^{tot}} \frac{n_{e,0}}{n_e} \frac{2R(\pi\rho_b^2 B_T)^2}{\frac{\partial V}{\partial \hat{\rho}}|\nabla\Phi|^2} \hat{\rho} e^{\frac{2}{3}\hat{\rho}^2(q_{95}+\frac{1}{2})}, \tag{41}$$

where the MHD safety factor at 95% flux surface is assumed to be $q_{95} = 3$ [23]. The profile $P_e^{tot}(\hat{\rho},t)$ is the total power (MW) enclosed within the magnetic-flux surface with mean-effective minor radius $\hat{\rho}$. It is found by solving

$$P_e^{tot}(\hat{\rho},t) = \int_0^{\hat{\rho}} Q_e^{tot}(\hat{\rho},t)\frac{\partial V}{\partial \hat{\rho}}(\hat{\rho})\partial\hat{\rho}, \tag{42}$$

at each value of $\hat{\rho}$. In (41), $P_{e,bdry}^{tot} = P_e^{tot}(1,t)$ at the boundary, $n_{e,0} = n_e(0,t)$ at the magnetic axis, Z_{eff} is the volume average of (10), $\nabla\Phi(\hat{\rho},t)$ is the gradient of Φ from (32), and $\hat{\rho}$ is the radial grid over the domain $0 \le \hat{\rho} \le 1$. The constants a_{121}, a_{122}, and α_n are tunable parameters [8]. In the transport equations (33) and (38), the ion thermal diffusion coefficient and the particle diffusion coefficients for the four ion species are assumed to be proportional to (41) such that $\chi_i(\hat{\rho},t) = \varrho_i \chi_e(\hat{\rho},t)$ and $D_p(\hat{\rho},t) = \mu_p \chi_e(\hat{\rho},t)$ for $p \in \{D, T, \alpha, I\}$. This work excludes the neoclassical contribution to χ_e (note that (41) models the anomalous contribution) due to the assumption that the anomalous contribution is much greater than the neoclassical contribution, which is supported by experimental observations [29].

6. 0-D burn control in 1-D space

As discussed in Section 1, the primary goal of burn control is the regulation of *volume-averaged* plasma properties, and recall from Section 3 that the proposed nonlinear burn controller is designed to track the volume-averaged references $r = [\bar{E}_i\ \bar{E}_e\ \bar{n}\ \bar{\gamma}]$. Therefore, the control laws for $P_{aux,i}$ (27), $P_{aux,e}$ (28), $S_{aux,D}$ (29) and $S_{aux,T}$ (30) are computed using volume-averaged quantities in a 1-D simulation. These control laws determine the value of the controlled inputs in the particle transport equations (33) and the heat transport equations (38): $\Gamma_D(\hat{\rho},t)$, $\Gamma_T(\hat{\rho},t)$, $Q_{aux,i}(\hat{\rho},t)$, and $Q_{aux,e}(\hat{\rho},t)$. Fig. 2 illustrates how the 0-D burn controller operates in 1-D plasma simulations.

In a 1-D simulation, the volume-averaged energies, densities, and source terms are found through integration:

$$E_j(t) = \frac{1}{V_p}\int_V \frac{3}{2} n_j(\hat{\rho},t) T_j(\hat{\rho},t)\partial V \quad \text{for} \quad j \in \{i, e\}, \tag{43}$$
$$n_j(t) = \frac{1}{V_p}\int_V n_j(\hat{\rho},t)\partial V \quad \text{for} \quad j \in \{D, T, \alpha, I\}, \tag{44}$$
$$P_j(t) = \frac{1}{V_p}\int_V Q_j(\hat{\rho},t)\partial V \quad \text{for} \quad j \in \{\alpha, ei, br, oh\}, \tag{45}$$
$$S_j(t) = \frac{1}{V_p}\int_V \Gamma_j(\hat{\rho},t)\partial V \quad \text{for} \quad j \in \{\alpha, sp\}, \tag{46}$$

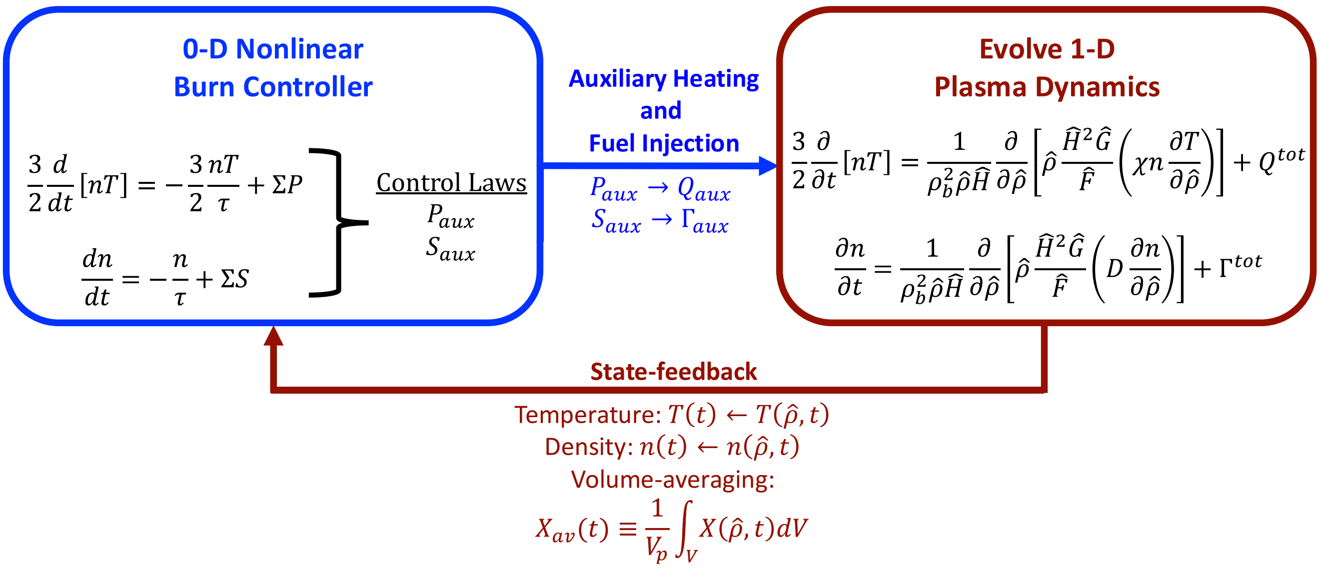

Fig. 2. This block diagram describes the framework for the closed-loop simulations presented in Section 7. Before the simulation, the control laws P_{aux} and S_{aux} (27)–(30) are synthesized from the 0-D plasma model: (1), (2), (11) and (12). In the 1-D simulation, the controller's heating and fueling commands map onto the controlled inputs Q_{aux} (48) and Γ_{aux} (49). These controlled inputs evolve the simulated 1-D plasma dynamics: (33) and (38). The loop is closed by taking the volume-average of the 1-D plasma quantities (43)–(46) and feeding them back to the burn controller. The control laws are computed using these volume-averaged quantities. Note that the subscripts that differentiate whether a quantity is related to the ion population, electron population or a particular ion species have been omitted from the diagram.

where V_p is the total plasma volume. In (27)–(30), the confinement time τ_E^{sc} is also computed using volume-averaged quantities. When solving (43)–(46), the volume average of quantity $X(\hat{\rho}, t)$ is rewritten as

$$X_{av}(t) = \frac{1}{V_p}\int_V X(\hat{\rho}, t)\partial V = \frac{1}{V_p}\int_0^1 X(\hat{\rho}, t)\frac{\partial V}{\partial \hat{\rho}}(\hat{\rho})\partial \hat{\rho}. \tag{47}$$

Once the controller's commands for $P_{aux,i}$, $P_{aux,e}$, $S_{aux,D}$ and $S_{aux,T}$ are determined, the controlled inputs into the 1-D transport equations are given by

$$Q_{aux,j}(\hat{\rho}, t) = P_{aux,j}(t) V_p \times \Lambda_{dep}(\hat{\rho}) \quad \text{for} \quad j \in \{i, e\}, \tag{48}$$

$$\Gamma_{aux,j}(\hat{\rho}, t) = S_{aux,j}(t) V_p \times \Lambda_{dep}(\hat{\rho}) \quad \text{for} \quad j \in \{D, T\}, \tag{49}$$

where $\Lambda_{dep}(\hat{\rho})$ is the radial deposition profile of the external heating and fueling. If $\Lambda_{dep}(\hat{\rho})$ is chosen such that $\int_V \Lambda_{dep}\partial V = \int_0^1 \Lambda_{dep}\frac{\partial V}{\partial \hat{\rho}}\partial \hat{\rho} = 1$ m^{-3}, then taking the volume average of $Q_{aux,j}(\hat{\rho}, t)$ from (48) gives $P_{aux,j}(\hat{\rho}, t)$:

$$\begin{aligned}\frac{1}{V_p}\int_V Q_{aux,j}(\hat{\rho}, t)\partial V &= \frac{1}{V_p}\int_V P_{aux,j}(t) V_p \times \Lambda_{dep}(\hat{\rho})\partial V \\ &= \frac{P_{aux,j}(t) V_p}{V_p}\int_V \Lambda_{dep}(\hat{\rho})\partial V = P_{aux,j}(t).\end{aligned} \tag{50}$$

Similarly, the volume average of $\Gamma_{aux,j}(\hat{\rho}, t)$ from (49) can be found to be $S_{aux,j}(\hat{\rho}, t)$.

7. Simulation study

In this section, the 0-D burn controller (Section 4) is tested in a 1-D simulation of the plasma model presented in Section 5. For this simulation, the radial profiles for $\hat{F}$, $\hat{G}$, $\hat{H}$, $\frac{\partial V}{\partial \hat{\rho}}$, and Λ_{dep} are shown in Fig. 3. For the proportionality between the various diffusion coefficients and χ_e (41), ϱ_i, μ_D, μ_T, μ_α, and μ_I were set to 1.2, 2, 3, 4, and 6, respectively. In addition, $\rho_b = 2.615$, $Z_I = 13$, $A_I = 27$, $f_I^{sp} = 0.01$, $a_{121} = 7.5 \times 10^9$, $a_{122} = 1.25 \times 10^{21}$, and $\alpha_n = 0.5$. The controller's initial estimate for each element of θ was set to 1. Finally, the boundary conditions for the 1-D transport equations (33) and (38) were set to be equal to $T_e^{bdry} = 0.1$ keV, $T_i^{bdry} = 0.1$ keV, $n_D^{bdry} = 7.76 \times 10^{18}$ m^{-3}, $n_T^{bdry} = 6.98 \times 10^{18}$ m^{-3}, $n_\alpha^{bdry} = 4.85 \times 10^{17}$ m^{-3}, and $n_I^{bdry} = 1.62 \times 10^{17}$ m^{-3}.

Because the proposed control design avoids linearization around a particular operating point, the controller can drive the plasma from one operating point to another. To show this in the simulation, the controller is tasked with tracking three different sets of volume-averaged references. Between $t = 50$ s and $t = 100$ s, the values for the references are set to be $E_i = 1.20 \times 10^5$ J/m^3, $E_e = 1.91 \times 10^5$ J/m^3, $n = 6.02 \times 10^{19}$ m^{-3}, and $\gamma = 0.5$. After $t = 100$ s the references are changed to $E_i = 1.23 \times 10^5$ J/m^3, $E_e = 2.30 \times 10^5$ J/m^3, $n = 6.25 \times 10^{19}$ m^{-3}, and $\gamma = 0.52$. Finally, the references are set to $E_i = 9.42 \times 10^4$ J/m^3, $E_e = 1.69 \times 10^5$ J/m^3, $n = 5.87 \times 10^{19}$ m^{-3}, and $\gamma = 0.45$ after $t = 150$ s.

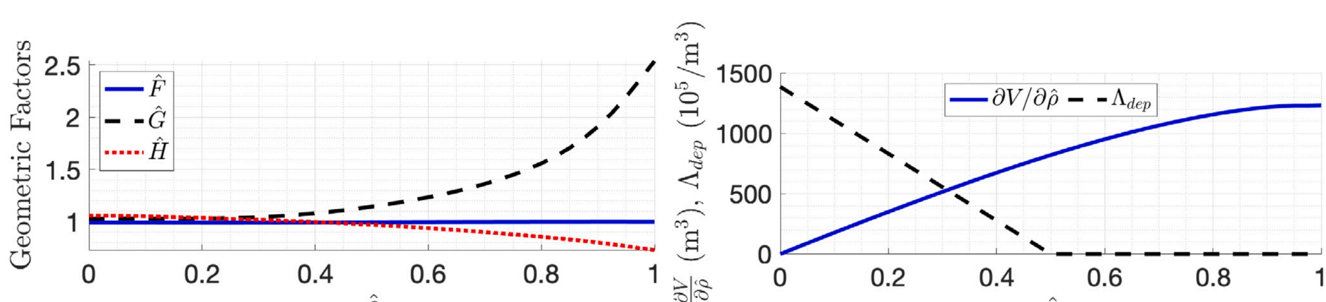

(a) Radial profiles for $\hat{F}$, $\hat{G}$, and $\hat{H}$

(b) Radial profiles for $\partial V/\partial \hat{\rho}$ and Λ_{dep}

Fig. 3. (a) Radial profiles for the geometric factors $\hat{F}$, $\hat{G}$, and $\hat{H}$. (b) Radial profiles for $\partial V/\partial \hat{\rho}$ and the actuator deposition Λ_{dep}.

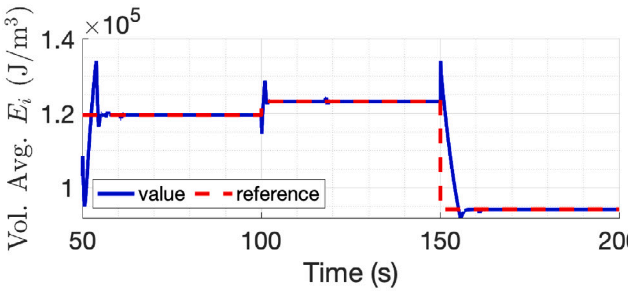

(a) Volume-averaged ion energy

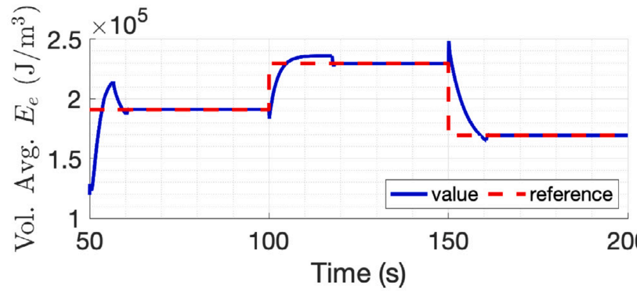

(b) Volume-averaged electron energy

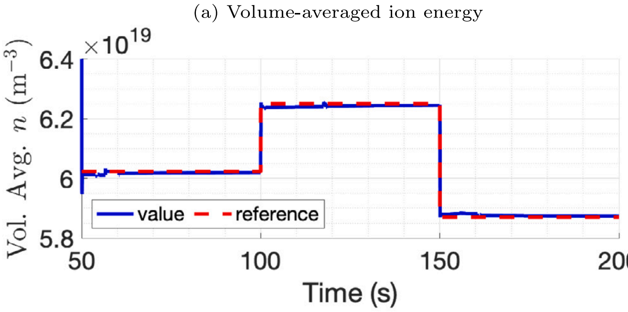

(c) Volume-averaged total plasma density

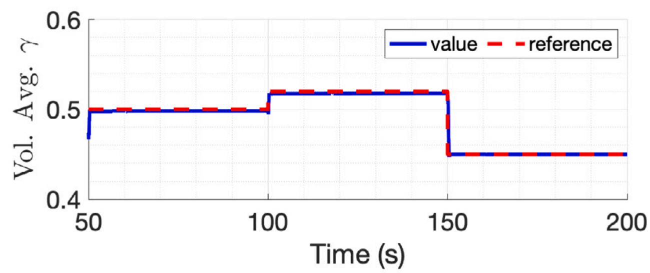

(d) Volume-averaged tritium fraction

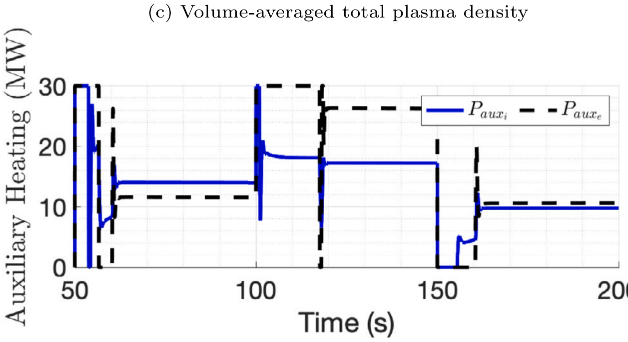

(e) Volume-averaged auxiliary power

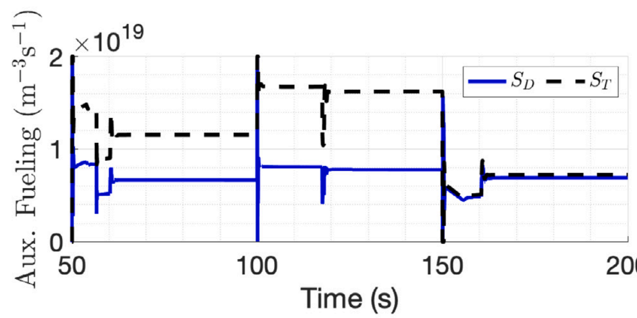

(f) Volume-averaged external fueling

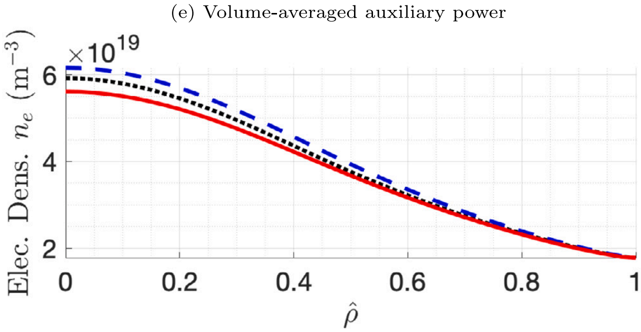

(g) Electron density profile

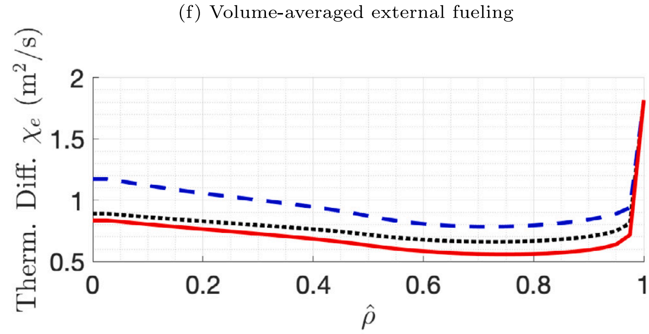

(h) Electron thermal diffusion coefficient profile

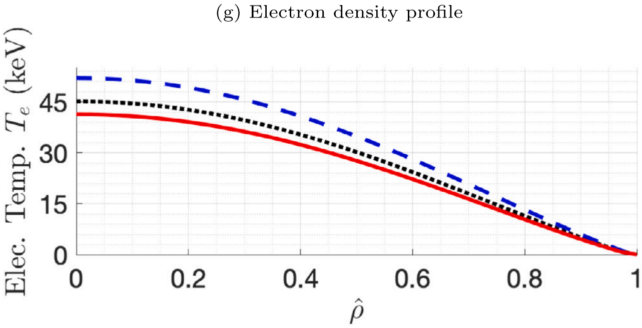

(i) Electron temperature profile

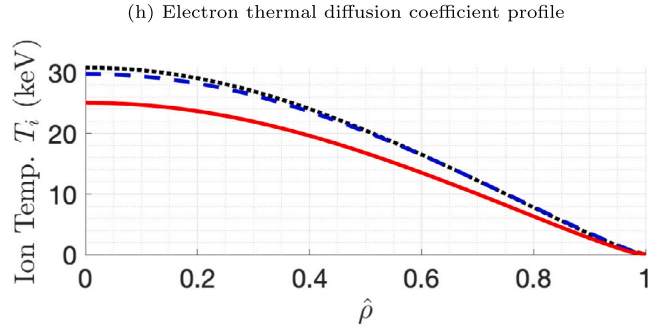

(j) Ion temperature profile

Fig. 4. (a)–(d) The nonlinear burn controller drives the volume-averaged quantities (solid-blue lines) to their reference values $r = [\bar{E}_i\ \ \bar{E}_e\ \ \bar{n}\ \ \bar{\gamma}]$ (red-dashed lines). (e)–(f) The burn controller's commands for external heating and fueling: $P_{aux,i}$, $P_{aux,e}$, $S_{aux,D}$, and $S_{aux,T}$. (g)–(j) The radial profiles for $n_e(\hat{\rho},t)$, $\chi_e(\hat{\rho},t)$, $T_e(\hat{\rho},t)$, and $T_i(\hat{\rho},t)$ at $t = 100$ s (black-dotted line), $t = 150$ s (blue-dashed lines), and $t = 200$ s (red-solid line). Note that the nonlinear burn controller receives new reference targets $r = [\bar{E}_i\ \ \bar{E}_e\ \ \bar{n}\ \ \bar{\gamma}]$ at $t = 100$ s and $t = 150$ s.

The results of this simulation are shown in Fig. 4. As shown in Fig. 4(a)–(d), the 0-D burn controller is able to track the volume-averaged references for E_i, E_e, n, and γ in the 1-D plasma simulation. The controller tracks the references by computing the necessary external heating and fueling from the control laws (27)–(30). The values of the control commands $P_{aux,i}$, $P_{aux,e}$, $S_{aux,D}$, and $S_{aux,T}$ are shown in Fig. 4(e)–(f). These control commands evolve the 1-D plasma system through the controlled inputs $Q_{aux,i}$, $Q_{aux,e}$, $\Gamma_{aux,D}$, and $\Gamma_{aux,T}$ as defined by (48) and (49). The evolution of the kinetic profiles is shown in Fig. 4(g)–(j). Specifically, the radial profiles for the electron density $n_e(\hat{\rho},t)$, the electron thermal diffusion coefficient $\chi_e(\hat{\rho},t)$, the electron temperature $T_e(\hat{\rho},t)$, and the ion temperature $T_i(\hat{\rho},t)$ are plotted at $t = 100$ s immediately before the references are swapped for the first time (black-dotted line), $t = 150$ s immediately before the references are swapped again (blue-dashed lines), and the end of the simulation $t=200$ s (red-solid line).

8. Conclusions and future work

In this work, a nonlinear burn controller was designed from the 0-D plasma dynamics presented in Section 2. In Section 7, this 0-D controller was used in closed-loop simulations of the 1-D plasma dynamics presented in Section 5. This simulation study demonstrated the capability of the controller in achieving its objectives in a 1-D environment. Also, it illustrated how the spatial profiles for temperature and density evolve temporally under 0-D burn control. While this work focuses on ITER, the 1-D model can be modified for present tokamaks, permitting the evaluation of kinetic control techniques ahead of an experiment.

The presented 1-D model can be used to assess various 0-D controllers from prior work, including those augmented with actuator allocators [5,30] that can optimally manage a suite of actuator systems (e.g., two neutral beam injectors, the ion and electron cyclotron systems, two pellet injectors, and the gas valves for ITER [16]). These actuator allocators were designed to handle actuator saturation and delays. Furthermore, observers that can estimate the plasma state with limited real-time measurements [31] can also be tested in 1-D simulations.

For future work, numerous improvements may be made to the 1-D burn control simulations. For example, the following items can be added to the model: a self-consistent equilibrium calculation, a temperature pedestal model, separate transport equations for the fast alpha-particles, and an improved model for the source of impurity particles. Furthermore, the particle diffusion coefficients could be modeled independently from the electron thermal diffusion coefficient (χ_e), and the transport models can be updated to include separate diffusion and convection terms. Finally, coupling the 1-D plasma model with models for the edge-plasma regions could enable integrated burn-divertor control simulations. For example, SOLPS parameterizations [17] or the two-point model [32] can provide boundary conditions for the transport equations (33) and (38) in addition to the divertor heat load. This work has already been completed for the 0-D plasma model [33,34].

In this work, the auxiliary heating and external fueling were assumed to have the identical radial deposition profiles (Λ_{dep} in Fig. 3(b)). To improve the 1-D simulations, future work will focus modeling more realistic deposition profiles for each of the different actuator systems. In addition, the actuator deposition profiles can be modeled as physics-based functions that change depending on the plasma conditions (e.g., pellet penetration may vary with changes in plasma density and temperature). Once each of the actuators are modeled with unique deposition profiles, future work may also include the control of kinetic profiles using 0-D burn control techniques. For plasma fueling, the gas fueling system's deposition profile will be limited to the plasma's edge, while the pellet fueling will penetrate further into the plasma's core. Therefore, these two actuators can be used in conjunction to control the density at two different radial positions. By controlling the density at two radial positions, the density profile can be shaped. Similarly, the temperature profile can be shaped by controlling the energy at two radial positions via neutral beam heating and off-axis electron cyclotron heating.

CRediT authorship contribution statement

Vincent Graber: Writing – review & editing, Writing – original draft, Visualization, Validation, Software, Methodology, Formal analysis, Conceptualization. **Eugenio Schuster:** Writing – review & editing, Visualization, Validation, Supervision, Software, Resources, Project administration, Methodology, Funding acquisition, Formal analysis, Conceptualization.

Declaration of competing interest

The authors declare that they have no known competing financial interests or personal relationships that could have appeared to influence the work reported in this paper.

Acknowledgments

This material is based upon work supported by the U.S. Department of Energy, Office of Science, Office of Fusion Energy under Award Number DE-SC-0010661, and it was carried out in part under the ITER Scientist Fellow Network program.

Data availability

The authors are unable or have chosen not to specify which data has been used.

References

[1] D. Humphreys, et al., Novel aspects of plasma control in ITER, Phys. Plasmas 22 (2) (2015) 021806.
[2] J. Wesson, Tokamaks, second ed., Clarendon Press, Oxford, 1997.
[3] Eugenio Schuster, Miroslav Krstić, George Tynan, Burn Control in Fusion Reactors Via Nonlinear Stabilization Techniques, Fusion Sci. Technol. 43 (2003).
[4] A. Pajares, E. Schuster, Robust nonlinear burn control in ITER to handle uncertainties in the fuel-line concentrations, Nucl. Fusion 59 (9) (2019).
[5] V. Graber, E. Schuster, Nonlinear burn control in ITER using adaptive allocation of actuators with uncertain dynamics, Nucl. Fusion 62 (2) (2022).
[6] H. Khalil, Nonlinear Systems, third ed., Prentice Hall, New Jersey, 2001.
[7] Krstić, et al., Nonlinear and Adaptive Control Design, Wiley, 1995.
[8] A. Pajares, et al., Optimization of parameterized transport models in COTSIM, in: 47th European Physical Society (EPS) Plasma Physics Conference, 2021.
[9] Brian R. Leard, et al., Fast model-based scenario optimization in NSTX-U enabled by analytic gradient computation, Fusion Eng. Des. 192 (2023) 113606.
[10] F. Felici, et al., Real-time-capable prediction of temperature and density profiles in a tokamak using RAPTOR and a first-principle-based transport model, Nucl. Fusion 58 (9) (2018) 096006.
[11] J.F. Artaud, et al., METIS: a fast integrated tokamak modelling tool for scenario design, Nucl. Fusion 58 (10) (2018) 105001.
[12] J.F. Artaud, et al., The CRONOS suite of codes for integrated tokamak modelling, Nucl. Fusion 50 (4) (2010) 043001.
[13] E. Fable, et al., The modeling of a tokamak plasma discharge, from first principles to a flight simulator, Plasma Phys. Control. Fusion 64 (4) (2022) 044002.
[14] L. Emanuel di Grazia, et al., Development of magnetic control for the EU-DEMO flight simulator and application to transient phenomena, Fusion Eng. Des. 191 (2023) 113579.
[15] G.V. Pereverzev, P.N. Yushmanov, ASTRA automated system for transport analysis, Max- Planck-Inst. Plasmaphys. (2002).
[16] J. Snipes, et al., Actuator and diagnostic requirements of the ITER plasma control system, Fusion Eng. Des. 87 (12) (2012).
[17] H.D. Pacher, et al., Impurity seeding in ITER DT plasmas in a carbon-free environment, J. Nucl. Mater. 463 (2015) 591–595.
[18] R.A. Pitts, et al., Plasma-wall interaction impact of the ITER re-baseline, Nucl. Mater. Energy 42 (2025) 101854.
[19] H. Bosch, G. Hale, Improved formulas for fusion cross-sections and thermal reactivities, Nucl. Fusion 32 (4) (1992).
[20] R. Gross, Fusion Energy, Wiley-Interscience, New York, 1984.

[21] D. Gallart, et al., Modelling of ICRF heating in DEMO with special emphasis on bulk ion heating, in: AIP Conf Proc, vol. 1689, 2015.
[22] V. Graber, E. Schuster, Nonlinear adaptive burn control and optimal control allocation of over-actuated two-temperature plasmas, in: American Control Conference, Denver, USA, 2020.
[23] M. Shimada, et al., Physics design of ITER-FEAT, J. Plasma Fusion Res. 3 (2000) 77–83.
[24] M. Shimada, et al., Chapter 1: Overview and summary, Nucl. Fusion 47 (2007).
[25] J. Barton, et al., Simultaneous closed-loop control of the current profile and the electron temperature profile in the TCV tokamak, in: American Control Conference, Illinois, USA, 2015.
[26] F.L. Hinton, R.D. Hazeltine, Theory of plasma transport in toroidal confinement systems, Rev. Modern Phys. 48 (2) (1976).
[27] W.M. Tang, Microinstability-based model for anomalous thermal confinement in tokamaks, Nucl. Fusion 26 (12) (1986) 1605.
[28] S.C. Jardin, M.G. Bell, N. Pomphrey, TSC simulation of ohmic discharges in TFTR, Nucl. Fusion 33 (3) (1993) 371.
[29] M. Erba, et al., Validation of a new mixed Bohm/gyro-Bohm model for electron and ion heat transport against the ITER, Tore Supra and START database discharges, Nucl. Fusion 38 (1998).
[30] V. Graber, E. Schuster, Actuator allocation with adaptive estimation of time-varying uncertain parameters for nonlinear burn control, in: IEEE Conference on Control Technology and Application, Trieste, Italy, 2022.
[31] Mark D. Boyer, Eugenio Schuster, Nonlinear burn control in tokamak fusion reactors via output feedback, IFAC Proc. Vol. 47 (3) (2014) 3702–3707, 19th IFAC World Congress.
[32] P.C. Stangeby, The Plasma Boundary, IOP, Bristol, 2000.
[33] V. Graber, E. Schuster, Assessment of the burning-plasma operational space in ITER by using a control-oriented core-SOL-divertor model, Fusion Eng. Des. 171 (2021).
[34] Vincent Graber, Eugenio Schuster, Divertor-safe nonlinear burn control based on a SOLPS parameterized core-edge model for ITER, Nucl. Fusion 64 (8) (2024) 086007.